Journal of Power Sources 196 (2011) 1940–1947

Contents lists available at ScienceDirect

Journal of Power Sources

journal homepage: www.elsevier.com/locate/jpowsour

Effects of a microporous layer on the performance degradation of proton exchange membrane fuel cells through repetitive freezing

Yongtaek Lee[a,1], Bosung Kim[a], Yongchan Kim[a,*], Xianguo Li[b]

[a] Department of Mechanical Engineering, Korea University, Anam-dong, Seongbuk-gu, Seoul 136-713, Republic of Korea
[b] Department of Mechanical and Mechatronics Engineering, University of Waterloo, Waterloo, Ontario N2L 3G1, Canada

ARTICLE INFO

Article history:
Received 7 July 2010
Received in revised form 7 October 2010
Accepted 8 October 2010
Available online 19 October 2010

Keywords:
Proton exchange membrane fuel cell
Microporous layer
Freezing
Degradation
Electrochemical impedance spectroscopy
Gas diffusion layer

ABSTRACT

The gas diffusion layer (GDL) covered with a microporous layer (MPL) is being widely used in proton exchange membrane fuel cells (PEMFCs). However, the effect of MPL on water transport is not so clear as yet; hence, many studies are still being carried out. In this study, the effect of MPL on the performance degradation of PEMFCs is investigated in repetitive freezing conditions. Two kinds of GDL differentiated by the existence of MPL are used in this experiment. Damage on the catalyst layer due to freezing takes place earlier when GDL with MPL is used. More water in the membrane and catalyst layer captured by MPL causes permanent damage on the catalyst layer faster. More detailed information about the degradation is obtained by electrochemical impedance spectroscopy (EIS). From the point of view that MPL reduces the ohmic resistance, it is effective until 40 freezing cycles, but has no more effect thereafter. On the other hand, from the point of view that MPL enhances mass transport, it delays the increase in the mass transport resistance.

1. Introduction

Water transport is one of the major research areas regarding proton exchange membrane fuel cells (PEMFCs). Water is essential to maintain the proton conductivity of the membrane but disturbs the gas transport to the catalyst layer at the same time. As water is generated at the catalyst layer, it is important to get rid of the water from the surface in a short time. The gas diffusion layer (GDL) plays a role in liquid and gas transport between the catalyst layer and the channel where the gas is flowing. GDL is a thin layer of porous media made up with bonded carbon fibers or woven carbon cloth. At high currents or high humidity, the water vapor generated at the catalyst layer is apt to condense to form a two-phase state. If the pores of GDL are hydrophilic, the water that fills the pores is not easily eliminated and blocks the pathways for gas transport. In order to prevent flooding, the GDL used in PEMFCs is generally treated with materials such as polytetrafluoroethylene (PTFE), thereby making a part of the pores hydrophobic. As the hydrophobic pores are not prone to be filled with water, the PTFE loading helps to maintain the pathways for gas from the channel to the catalyst layer.

When water is formed at the catalyst layer, it will instantaneously occupy the adjacent empty hydrophilic pores. However, after all the hydrophilic pores are occupied by water, no more water can be absorbed by GDL. This is because the water inside the pores will not move through the pore network without the pressure difference that can overcome the surface tension of water on the hydrophilic surface. It was thought that the attachment of a microporous layer (MPL) composed of very highly hydrophobic material could enhance water transport through GDL, and a lot of studies have been carried out about the effects. These studies focused on the composition of MPL, experimental evaluation of the effect, and modeling of water transport in the MPL. Qi et al. [1] inserted a PTFE/carbon sublayer between the carbon paper and the catalyst layer. They differentiated the sublayer in terms of the content of PTFE and showed that a sublayer containing 35% of PTFE yielded the best performance. They also suggested that a sublayered GDL offers better performance than a non-sublayered GDL at high current densities. The same effect was reported by Chen et al. [2] and Park et al. [3]. Pasaogullari and Wang [4] studied two-phase transport in porous layers in the cathode with a multi-phase mixture model (M^2) to suggest that MPL enhances liquid-water removal and reduces liquid saturation in the catalyst layer. However, upon consideration of the membrane in the model, MPL was found to have a significant impact on the membrane. Weber and Newman [5] showed experimental results for two kinds of GDL to verify their simulation data. According to their results, the performance of GDL with MPL was much higher than that of GDL without MPL. They also

* Corresponding author. Tel.: +82 2 3290 3366; fax: +82 2 921 5439.
E-mail address: yongckim@korea.ac.kr (Y. Kim).
[1] Current address: Department of Mechanical and Mechatronics Engineering, University of Waterloo, Waterloo, Ontario N2L 3G1, Canada.

0378-7753/$ – see front matter © 2010 Elsevier B.V. All rights reserved.
doi:10.1016/j.jpowsour.2010.10.028

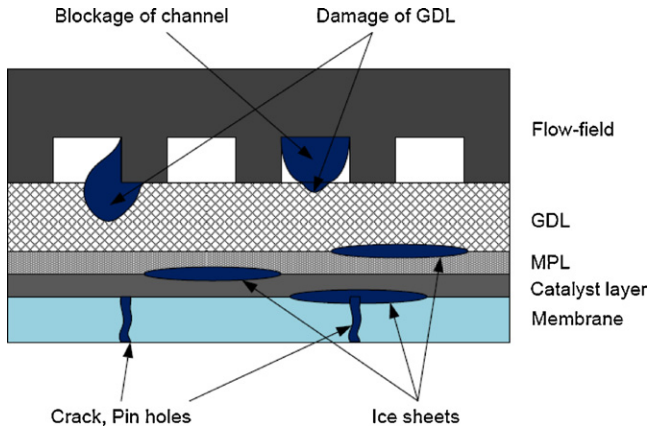

Fig. 1. Conjectured mechanism of degradation of PEMFCs in freezing conditions.

insisted that MPL keeps water out of the cathode GDL and moves it through the anode. The back flow of water to the anode through the membrane was also suggested by Pasaogullari et al. [6]. On the other hand, some papers report different findings. Williams et al. [7] and Lim and Wang [8] showed that GDL with MPL caused a higher performance drop at high current densities. According to Williams et al. [7], a GDL with higher gas permeability has a higher limiting current. This means that GDL without MPL has a higher limiting current, thereby being profitable at high current densities. In addition, Atiyeh et al. [9] tried to experimentally measure the effect of MPL on the net water drag coefficient through the membrane but found no effect on the drag coefficient. The role of MPL in water transport is not so clear as yet; hence, many studies are still being carried out.

The degradation of PEMFCs caused by the freezing of water inside is another big issue in PEMFC research. While the cell is operating, the heat from the chemical reaction and ohmic heating can maintain the cell temperature at the desired point even in very cold environments. However, after the operation ends, the fuel cell exposed to the cold weather cannot prevent the freezing of inside water. Fig. 1 shows the presumed mechanism of the degradation of PEMFCs in freezing conditions. The water can exist everywhere inside a PEMFC even after the operation is finished. The water can remain in the membrane, catalyst layer, GDL, and gas-flow channel. As the PEMFC is cooled down below the freezing temperature, the water inside begins to freeze thereby forming ice sheets or ice balls. The expansion of volume during freezing can give rise to some mechanical damage to the components of the PEMFC [10]. At first, the ice formation can cause pinhole damage or microcracking on the surface of the membrane, which causes hydrogen crossover, thereby reducing the OCV. The ice sheet formation on the catalyst layer also can delaminate the catalyst layer from both the membrane and GDL. This delamination reduces electron and proton conductivity. GDL also can be damaged by ice formation. The deformation of pores brings about the detachment of the PTFE coating from the carbon fibers. It causes the fracture of the carbon fibers and the binding material as well. Finally, ice columns or ice balls in the channel can cause damage to the surface of GDL. In addition, if the PEMFC starts to run before the ice melts, local starvation of fuel and air can happen because the ice blocks the flow of gases through the channel.

Several studies deal with the degradation of PEMFCs through freezing. Cho et al. [11] observed the performance degradation of PEMFCs after only four freeze/thaw cycles, and they reduced the degradation by applying dry-gas purge and anti-freeze solutions in their succeeding studies [12]. Hou et al. [13] applied humid gas purging and demonstrated no loss in performance after 20 cycles. It was suggested that the performance gradient is due to the reduction of the catalyst surface area by cyclic voltammetric measurement [11–14]. Kim et al. [15,16] observed the physical degradation of the catalyst layer under freeze/thaw cycles using scanning electron microscope (SEM). However, the degradation mechanism is too complicated to be explained by just a few factors as shown in Fig. 1. Moreover, considering that the studies were carried out in the region of relatively low current, the effect of mass transport may have been ignored.

As mentioned in previous papers, ice formation near the catalyst layer plays a major role in the performance degradation of PEMFCs. The water near that area is mainly determined by MPL. Thus, the presence of MPL can affect the characteristics of degradation caused by freezing. In addition, the change in the characteristics of MPL due to freezing may have a large impact on the mass transport of reactant gases. However, to the best of the authors' knowledge, no former studies have dealt with the effect of MPL in freezing conditions. No prior research has offered any quantitative results related to the degradation of the mass transport characteristics of operating PEMFCs. In this study, the comparison of degradation characteristics of PEMFCs using two different kinds of GDL was performed to observe the effect of MPL. Especially, the variation of the mass-transport loss according to the presence of MPL was evaluated quantitatively by electrochemical impedance spectroscopy (EIS).

2. Experimental

2.1. Experimental setup

The PEMFC used in this experiment was designed for a water cooling system even though a unit cell was employed. Different from other studies that used a constant-temperature chamber to freeze the cell, this work forced anti-freeze to flow inside the end plates to control the temperature of the cell. Fig. 2 shows

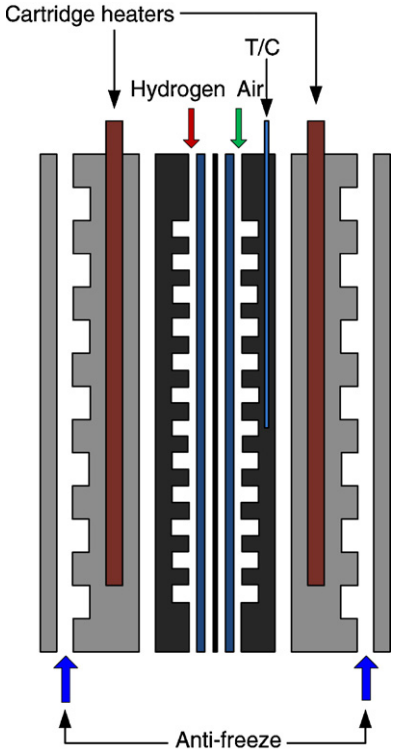

Fig. 2. Schematic diagram of the cell assembly.

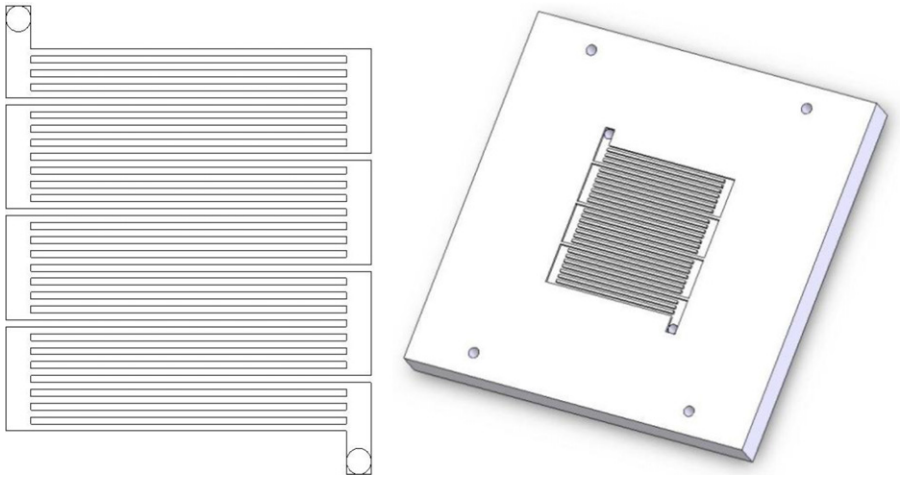

Fig. 3. Configuration of the modified serpentine-type flow-field for the reactant gases and a 3D image of the separator.

a schematic diagram of the cell assembly. Each end plate was composed of two stainless steel plates. The flow channel for the anti-freeze was machined on one of them and covered with the other flat plate. The two plates were blazed in a furnace to seal the gaps between the plates on not only the perimeter but also the land area between the channels. A T-type thermocouple was located at the center of the cathode side flow-field plate to measure the temperature of the cell. Because the heat generation rate from a unit PEMFC is not very high, additional electric heaters are demanded. A cartridge heater inserted in each end plate was used while the cell was operating as well as being heated up.

This study used a four-channel, modified serpentine-type flow-field, as shown in Fig. 3. Gore^{TM}'s 57 series MEA with the active area of 25 cm^2 was employed. The GDLs used in this work were GDL 10BA and GDL 35BC. GDL 35BC is composed of two layers, a MPL and a substance with coarse pores. The substance was hydrophobically treated with 5 wt% of PTFE. GDL 10BA has the same structure and PTFE loading as those in the case of GDL 35BC but has no MPL.

Fig. 4 shows a schematic diagram of the overall experimental setup to measure the performance of the PEMFC in freezing conditions. The flow rate of reactant gases was controlled by the mass flow controllers (MFCs) of the test station. Two sparging-type humidifiers were used to control the humidity of the reactant gases. The humidity was determined by the temperature of the humidifier and the temperature of the cell, as described in our former papers [17,18]. The temperature of the PEMFC was maintained at

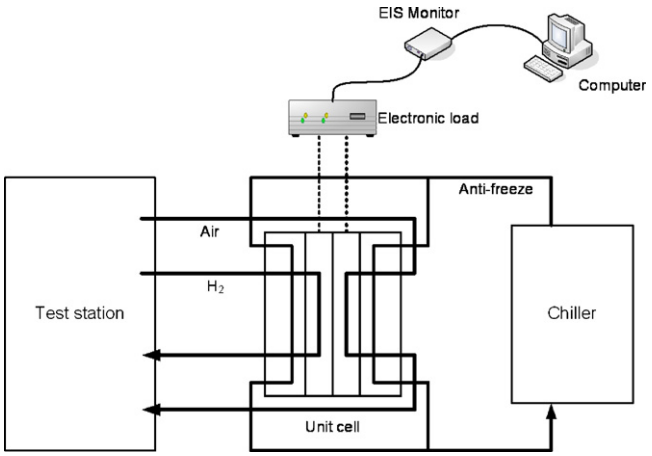

Fig. 4. Schematic diagram of the experimental setup.

the set temperature by adjusting the flow rate and the temperature of the anti-freeze through the end-plates. The temperature of the anti-freeze was controlled by using a chiller that could cool down the anti-freeze to below −20 °C. The electrochemical characteristics of the PEMFC were measured by EIS. A Gamry FC350^{TM} fuel cell monitor and a TDI electronic load (RLB 488 50-150-800) were employed for the EIS measurement. The sweeping frequency ranged from 10 mHz to 20 kHz.

2.2. Test conditions

The polarization curves were obtained at 60%, 80%, and 100% RH. Both hydrogen and air were humidified at the same humidity. EIS was carried out at 80% and 100% RH. The stoichiometries for air/H_2 were maintained at 2.5/1.5. During the EIS measurement, to reduce the instability of the voltage, the stoichiometry of air was slightly increased (3/1.5). Before the first freezing cycle, the polarization curves and EIS data were obtained at every humidity condition under a cell temperature of 70 °C. After the operation, the anti-freeze flew into both end plates, and the cell was cooled down. When a cell at 70 °C suddenly makes contact with anti-freeze at −20 °C, there may be unexpected damage to the PEMFC. To prevent thermal shock, the cell was cooled down in the ambient environment until the temperature dropped to 40 °C. Then, the anti-freeze whose temperature is around 0 °C started to flow into the flow channel inside the end plate at a very low flow rate. At the same time, the chiller started to cool the anti-freeze down to −20 °C. The flow rate of the anti-freeze increased slowly until the temperature of the cell reached 10 °C, thereafter reaching its terminal value of 0.04 m^3 h^{-1}. After the temperature reached −15 °C, the cell was maintained at that temperature for 2 h. As mentioned in the prior literature [12,13,19,20], the degradation of PEMFCs by freezing is very sensitive to the purging effect. If there was undesired purging of water from the cell, it could affect the results of this experiment. Therefore, to eliminate the purging effect, the valves at the inlet of the cell were closed at the same time as the stoppage of drawing current from the cell.

After 2 h' freezing, the cell was melted at room temperature. The operation was not restarted until the temperature of the cell rose above 10 °C, where the ice inside of the cell was judged to have been melted. Then, we drew 0.6 A cm^{-2} from the PEMFC to heat the cell with the heater until it reached a steady state at 70 °C and 100% RH. The performance of the cell was measured by varying current density (j) from 0 to 1 A cm^{-2}. After operating for about 2 h, the cell went through the freezing process again. After several freezing

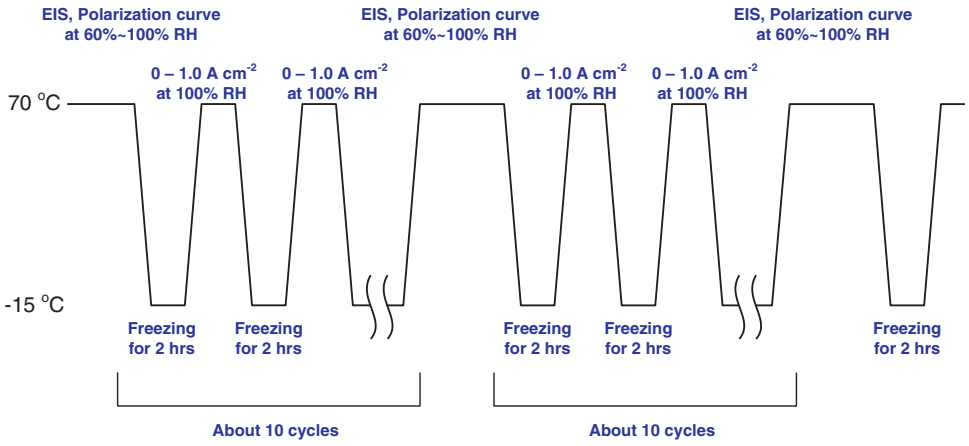

Fig. 5. Procedure of the experiment.

cycles, the polarization curves and the EIS results were obtained at 80–100% RH. Fig. 5 shows the procedure of the experiment.

3. Results and discussion

3.1. Performance degradation with freezing cycles

Performance degradation was observed as the freezing cycles progressed. Fig. 6 shows the voltage variation of the PEMFC using GDL 10BA with the number of freezing cycles. The humidities of hydrogen and air were 100% and the voltages were measured at the current densities of 0, 0.4, 0.8, and 1.0 A cm^{-2}, respectively. The rate of degradation of the performance at each current density was represented with a linear regression line. The rate of voltage reduction increased in magnitude as the current density increased. At OCV and j = 0.4 A cm^{-2}, the voltage changed little through the 23 cycles. The voltage degradation at OCV and low current densities is mainly attributed to the damage of the membrane such as cracks or pin holes that can yield gas cross-over between the anode and cathode. Thus, only a slight voltage variation indicates that the membrane itself was not damaged much by repetitive freezing cycles. However, as the current density increased to j = 0.8 and 1.0 A cm^{-2}, the gradient of degradation showed quite high values as $\Delta mV/\Delta n = -2.3$ and -3.2, respectively. The degradation can be regarded as being caused by increases in the charge transfer resistance and mass transfer resistance due to the freezing of water.

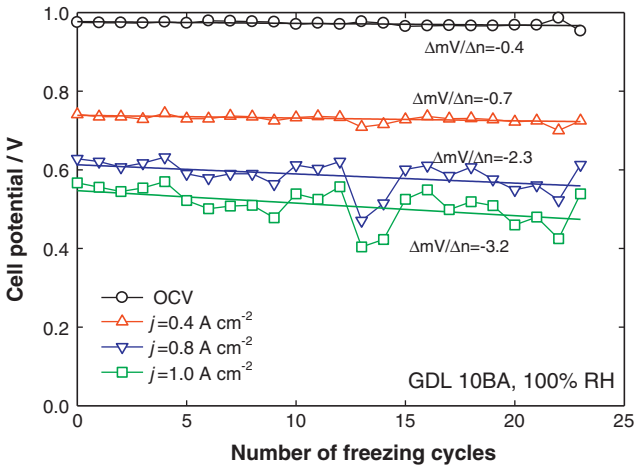

Fig. 6. Performance variation of the PEMFC with GDL 10BA with the number of freezing cycles.

The performance reduction did not occur at every cycle of freezing. While the performance was decreasing on the whole, it fluctuated with the number of freezing cycles like a wave. This phenomenon can be explained through the recovery of the catalyst area. As shown in Fig. 7, water can be located in the open pores between the carbon substrate and the ionomer. Water can also remain between Pt particles and the ionomer since the ionomer is very hydrophilic. When such water freezes, the expansion of ice can separate the Pt particles from the ionomer, thereby leading to a reduction in the effective Pt area. Such a reduction in the Pt area causes a decrease in the performance [11–14]. Even when the temperature rises above the freezing temperature, the melted water is not easily eliminated. The water trapped between the Pt particles and the ionomers disturbs the transport of protons. Ge and Wang [14] revealed that a high cell temperature can remove the water trapped inside the catalyst layer by evaporation, thus recovering the performance. However, the recovery process cannot restore the performance to that just before freezing. The accumulation of irreversibility under repetitive freezing causes permanent degradation of the PEMFC. In this work, the recovery operation was not performed additionally. Thus, the difference in the process of reheating caused a fluctuation in the performance under repetitive freezing.

Fig. 8(a) and (b) shows the polarization curves for the PEMFC with GDL 10BA at relative humidities of 60% and 100%, respectively.

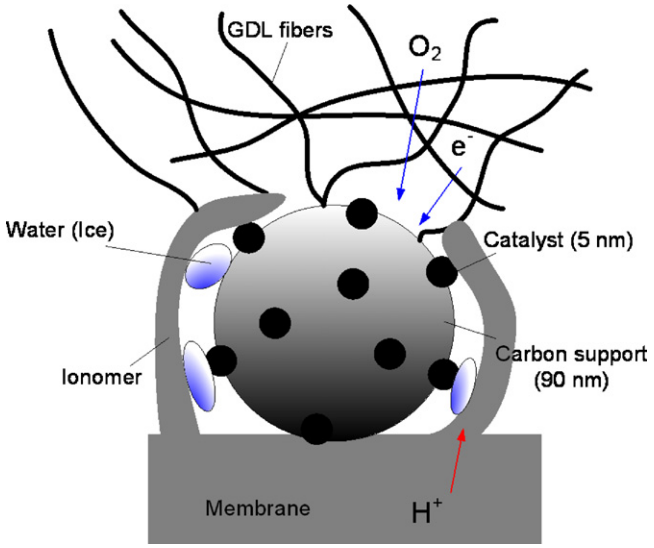

Fig. 7. Schematic of ice formation and distribution at the catalyst layer at the micro-scale.

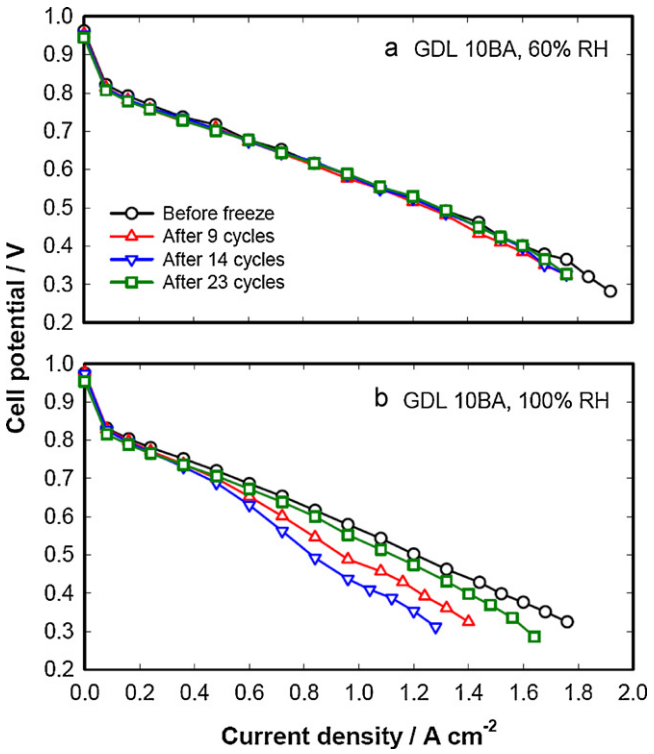

Fig. 8. Polarization curves of the PEMFC with GDL 10BA: (a) at $\varphi = 60\%$ and (b) at $\varphi = 100\%$.

In Fig. 8(a), when the relative humidity was 60%, the voltage varied very small as the thermal cycle progressed. Whereas at $\varphi = 100\%$, the performance degraded considerably. This degradation was not consistent with an increase in the number of freezing cycles. This corresponds to the fluctuation of the performance shown in Fig. 6. There was no degradation after 23 freezing cycles at $\varphi = 60\%$, but there was significant degradation at $\varphi = 100\%$. This implies that the degradation of the performance for the PEMFC with GDL 10BA is substantially attributed to the increase in the mass transport resistance.

Fig. 9 shows the voltage variation with the number of freezing cycles of a PEMFC using GDL 35BC, which has MPL on the surface facing the catalyst layer. Similar to GDL 10BA, the membrane was not damaged by freezing cycles judging from the slight OCV reduction. The rate of change was also represented by linear regression due to the fluctuation of the voltage with the number of freezing cycles. As the current density increased, the degradation of the performance was accelerated more than that of GDL 10BA. At $j = 1.0\ \mathrm{A\,cm^{-2}}$, the gradient of the voltage, $\Delta mV/\Delta n$, was 26% higher in magnitude than that of GDL 10BA. Considering that the gradient of the voltage reduction for GDL 35BC was lower at current densities of 0.4 and $0.8\ \mathrm{A\,cm^{-2}}$, the degradation of the performance of GDL 35BC was more severe under high current densities.

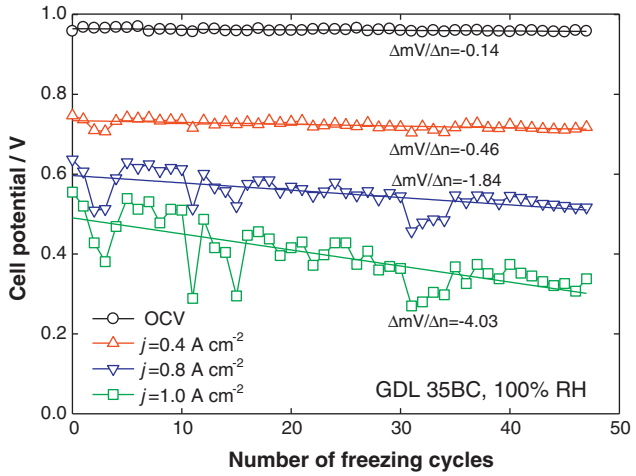

Fig. 9. Performance variation of the PEMFC with GDL 35BC with the number of freezing cycles.

It is noticeable from Figs. 6 and 9 that the fluctuation of the performance regarding GDL 35BC reduced with the number of freezing cycles, while it increased for GDL 10BA. Considering that the fluctuation of the performance arises from the damage and recovery of the catalyst layer, this result indicates that the possibility for permanent damage on the catalyst layer increases earlier for GDL 35BC. However, it cannot be concluded from these results that the rate of degradation on the catalyst layer due to the effective Pt area loss is higher for the PEMFC with GDL 35BC.

Fig. 10(a) and (b) shows the polarization curves for the PEMFC with GDL 35BC. As the relative humidity increased from 60% to 100%, the degradation of the performance in accordance with freezing cycles was intensified as in the case of GDL 10BA (Fig. 8). However, the magnitude of the degradation in the PEMFC with GDL 35BC was smaller than that in the PEMFC with GDL 10BA. This means that the mass transport loss of GDL 35BC did not increase so much as that of GDL 10BA for 40 freezing cycles.

As shown in Fig. 10(a) and (b), the performance reduction between "before freeze' and "after 16 cycles" was much larger than that between "after 16 cycles" and "after 27 cycles". This implies that the permanent damage on the catalyst layer such as the loss of effective Pt area takes place at the early freezing cycles and only a small amount of degradation occurs afterwards. This trend corresponds to the fact that the fluctuation of the performance according to the freezing cycles decreased after 16th freezing cycle (Fig. 9). As mentioned in Refs. [5,6], the effect of MPL is to push the water

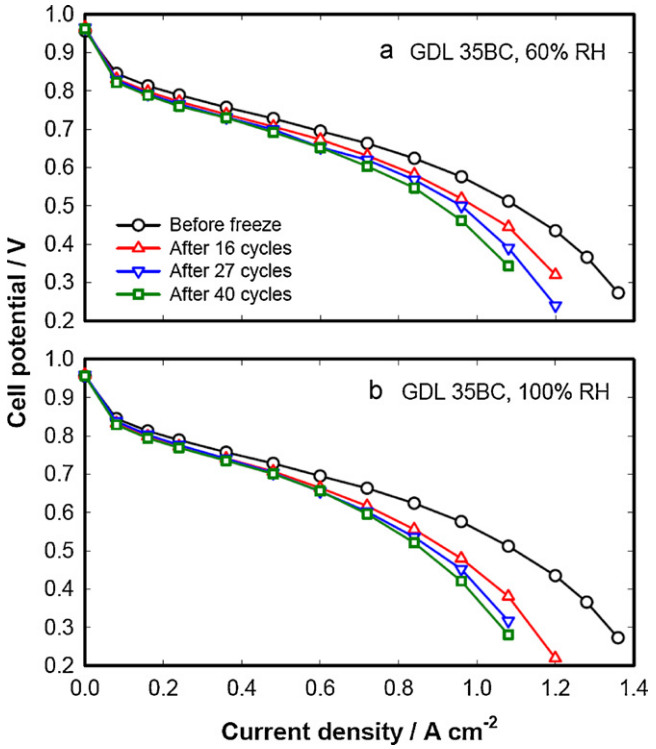

Fig. 10. Polarization curves of the PEMFC with GDL 35BC: (a) at $\varphi = 60\%$ and (b) at $\varphi = 100\%$.

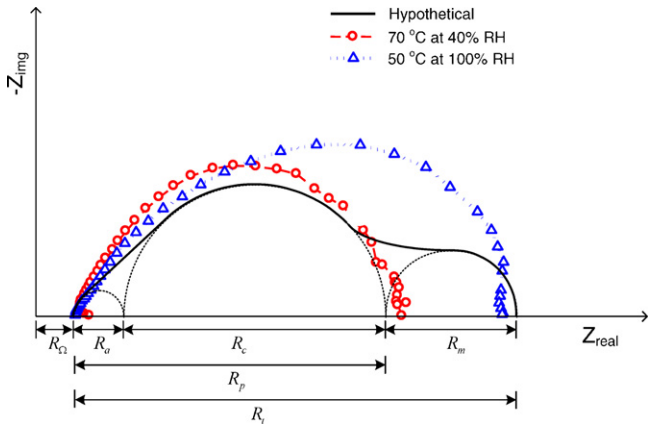

Fig. 11. Nyquist plots of hypothetical and actual PEMFCs referred from [18].

toward the anode as well as flow-field channel. Hence, more water will stay in the membrane and catalyst layer after finishing the operation of the PEMFC, when GDL with MPL is applied. This yields more damage on the catalyst layer.

3.2. Interpretation of the EIS results

The variation of the performance according to the repetitive freezing cycles was observed in the previous section. However, it provides insufficient information about the degradation mechanism. Thus, Nyquist plots were introduced to analyze the individual factors that cause performance degradation using the electrochemical characterization technique. In addition, the external humidification condition for the supplied gases was varied to observe its effect on the EIS results.

Fig. 11 shows the Nyquist plots of a hypothetical PEMFC and an actual PEMFC. In the hypothetical plot, R_Ω represents the total ohmic resistance for all components of the fuel cell. All ohmic resistances of the current collectors, flow-field plates, the membrane, and catalyst layers, and the contact resistance between components are included in R_Ω. The polarization resistance, R_p, is the sum of the anode activation loss (R_a) and the cathode activation loss (R_c). The last semicircle in the hypothetical Nyquist plot shows the mass transfer effect, R_m, which occurs in the low frequency region. The distance between the first and second interception points of the hypothetical Nyquist plot with the x-axis includes the polarization resistance, R_p, and the mass transfer effect, R_m. The actual Nyquist plots, which have triangular and circular symbols, were obtained in our previous study [18] using the same PEMFC and EIS monitor. When the mass transfer effect was insignificant (cell temperature of 70 °C and 40% RH), a small semicircular Nyquist plot containing only R_p, which is represented by circular symbols in Fig. 11, was observed. However, when the mass transfer effect was substantial (cell temperature of 50 °C and 100% RH), a large distorted semicircle containing R_p and R_m was observed, as represented with the triangular symbols in Fig. 11. Generally, the low-frequency semicircle, R_m, becomes indistinct at high stoichiometry. The two semicircles overlap thereby yielding a distorted semicircle, as shown with the triangular symbols in Fig. 11 [18,23,24]. The distance between the two intercepts on the Nyquist plot with the x-axis was defined as the total polarization resistance, R_t, which includes the activation and mass transport resistances.

Fig. 12(a)–(d) illustrates Nyquist plots for GDL 10BA at 80% RH and 100% RH. The figures show the variation of Nyquist plots obtained before freezing, and after 9, 14, and 23 freezing cycles, respectively. The diameter of the semicircle, i.e., total polarization resistance, R_t, varies with the repetitions of freezing. The Nyquist plots did not show large variations at $j = 0.2\ \mathrm{A\,cm^{-2}}$, while

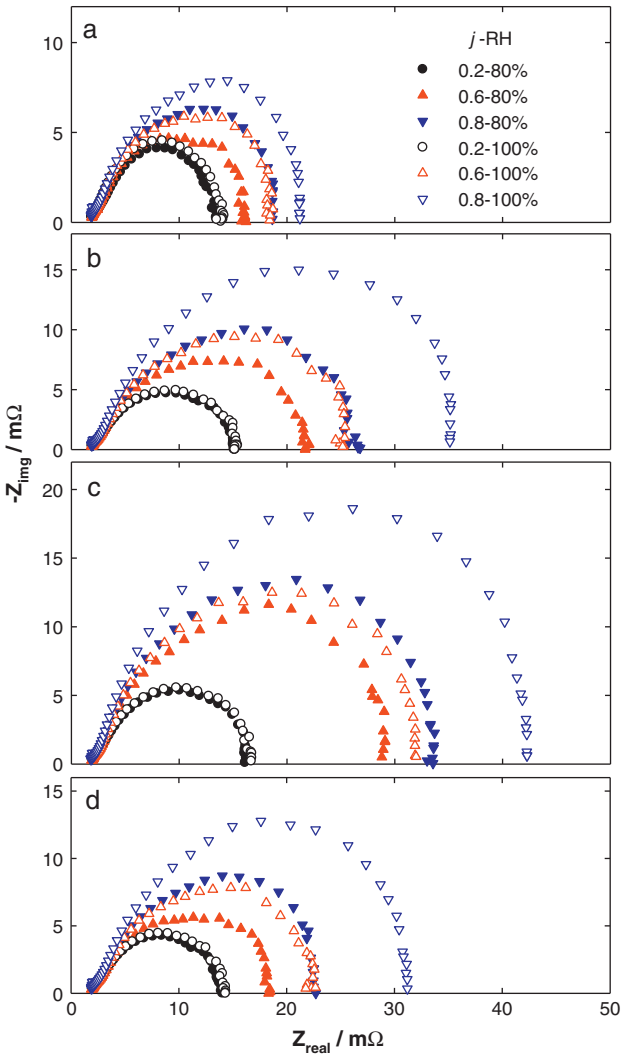

Fig. 12. Nyquist plots of the PEMFC with GDL 10BA according to the current density and relative humidity: (a) before freezing, (b) after 9 freezing cycles, (c) after 14 freezing cycles, and (d) after 23 freezing cycles.

R_t increased with the number of freezing cycles at $j = 0.6$ and $0.8\ \mathrm{A\,cm^{-2}}$. The results correspond with those of Fig. 6 in which the performance for low current densities showed little degradation, and the degradation was intensified with increasing current density. It can be seen from Fig. 12(d) that R_t reduced after 23 freezing cycles, while it kept rising in Fig. 12(a)–(c). This owes to the same reason as for the performance fluctuation that was observed in Fig. 6.

As the current density increased, the size of the semicircles increased. Generally, the diameter of the Nyquist plot decreases with increasing current density in the low current region where there is no mass-transport effect. However, Fig. 12 shows that R_t increased when the current density varied from 0.2 to $0.8\ \mathrm{A\,cm^{-2}}$. Thus, it can be estimated that the semicircles at $j = 0.6$ and $0.8\ \mathrm{A\,cm^{-2}}$ already contain the mass transport effect, R_m, within themselves [18,21–23].

Another factor that affects the Nyquist plots is the relative humidity. R_t increased as the relative humidity varied from 80% to 100%. While the variation of R_t due to the RH change was negligible at $0.2\ \mathrm{A\,cm^{-2}}$, it became larger with increasing current density. It can be inferred that the interruption of gas access to the catalyst layer by water flooding is the reason for the increasing R_t because a high current density accompanies a high rate of water generation

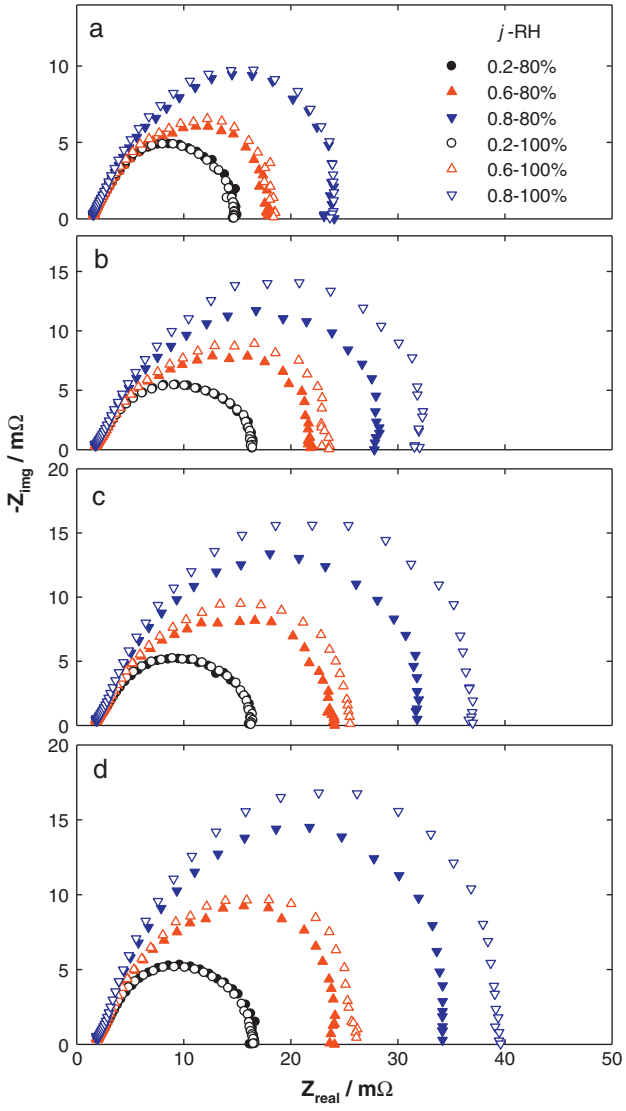

Fig. 13. Nyquist plots of the PEMFC with GDL 35BC according to the current density and relative humidity: (a) before freezing, (b) after 16 freezing cycles, (c) after 27 freezing cycles, and (d) after 40 freezing cycles.

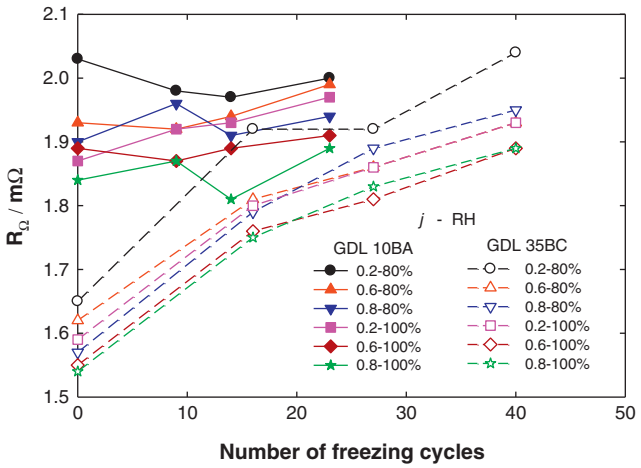

Fig. 14. Variation of R_Ω with the number of freezing cycles.

that simultaneously requires a high feeding speed of gases.

Fig. 13 shows the Nyquist plots for GDL 35BC. Similar to GDL 10BA, R_t increased with repetitive freezing cycles, increasing current density, and increasing relative humidity. However, by comparing with the Nyquist curves in Fig. 12, it is seen that the variation of R_t according to increasing RH was less. Especially before freezing, the two curves representing 80% RH and 100% RH coincide with each other. The MPL, which was the only difference between GDL 10BA and GDL 35BC, reduced the increase of R_t when the relative humidity changed from 80% to 100%, which indicates that MPL has a positive effect on the mitigation of flooding.

To analyze the result of EIS in more detail, the variations of the ohmic resistance (R_Ω) and total polarization resistance (R_t) were investigated separately from the Nyquist plots. It is not easy to perceive the variation of R_Ω from Figs. 12 and 13. Even though the change in R_Ω is small and has only a slight effect on the variation in the performance, it is worth looking closely at the variation of R_Ω to characterize the effect of MPL. Thus, the values of R_Ω for all the experimental cases were plotted, as shown in Fig. 14. The PEMFC using GDL 10BA showed higher R_Ω than GDL 35BC before freezing. MPL reduces the contact resistance between the catalyst layer and GDL, enhancing the conductivity. Moreover, the proton conductivity of the membrane can increase as the water at the surface of the catalyst later of the cathode is pushed toward the anode side by the high capillary pressure of MPL.

R_Ω showed various values according to the current density and relative humidity. It decreased as the current density and humidity rose. Regardless of the kind of GDL, it showed the highest R_Ω at $j = 0.2\ \mathrm{A\,cm^{-2}}$ and 80% RH where the membrane was prone to be the most dehydrated and the lowest at $j = 0.8\ \mathrm{A\,cm^{-2}}$ and 100% RH, where the membrane was prone to be the most hydrated. The difference in R_Ω between the two kinds of GDL is the variation with repeated cycles. R_Ωs of GDL 10BA did not show any specific trend in the change. However, R_Ωs of GDL 35BC increased with repeated cycles. It may be inferred that the contact resistance increased owing to the ice formation between the catalyst layer and MPL. Another possible means of R_Ω reduction is the decreased membrane hydration. If cracks develop in MPL accordingly reducing the contact area between MPL and catalyst layer, the back-flow of water through the membrane due to the high capillary pressure in the small pores of MPL will be reduced. Consequently, the reduction of membrane hydration causes an increase of R_Ω.

As the variation of the ohmic resistance according to the number of cycles is relatively small, the performance variation is wholly elucidated by the variation of the total polarization resistance, R_t, which is composed of R_p and R_m. As the main role of MPL is to enhance water transport through the GDL and mitigate flooding, an investigation is required into the variation of the mass transport resistance. However, the effect of the mass transport resistance is not distinguishable in the Nyquist plots from this work. Even if it was shown in the plot, it would be not easy to obtain quantitative values for the mass transport resistance, R_m. Thus, a new parameter was induced to express the effect of the mass transport loss. From Figs. 12 and 13, it could be seen that R_t changed much when the relative humidity increased from 80% to 100%. The increment of R_m was defined as shown in Eq. (1).

$$\Delta R_m = R_{t,100\%} - R_{t,80\%} \tag{1}$$

For this evaluation, it is necessary to assume that the variation of R_p has no relation to the humidity variation. Actually, R_p is also affected by the humidity, but according to our previous study [18], R_t varies only a little as the relative humidity varies from 80% to 100% when the current density is small (wherein the effect of R_m is minimal). Thus, the change in R_p can be assumed to be negligible compared with that of R_m. Fig. 15 shows the variation of ΔR_m for two kinds of GDL and three current densities according to the repeated freezing cycles. At $j = 0.2\ \mathrm{A\,cm^{-2}}$, ΔR_m showed a small

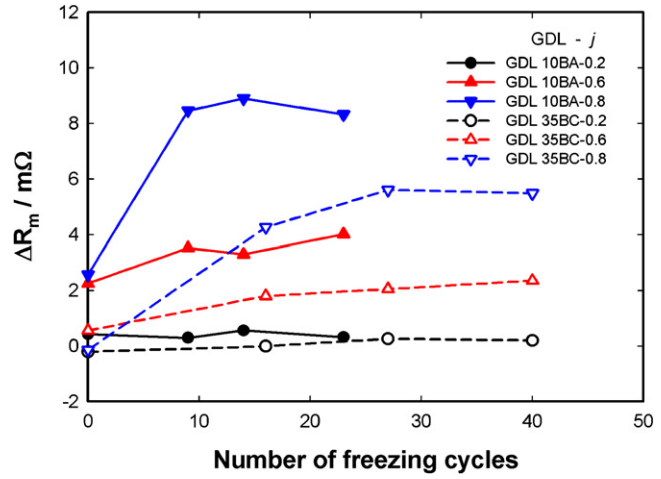

Fig. 15. Variation of ΔR_m with the number of freezing cycles.

absolute value and little variation for both GDLs. At $j = 0.6\ A\ cm^{-2}$, ΔR_m increased slightly, viz., 1.76 mΩ for GDL 10BA and 1.79 mΩ for GDL 35BC after 23 and 40 freezing cycles, respectively. Remarkable results can be observed at a high current density ($j = 0.8\ A\ cm^{-2}$). ΔR_m for GDL 10BA increased a lot during the early freezing cycles. It increased from 2.56 mΩ to 8.46 mΩ after the first nine cycles. After the ninth cycle, it showed little variation during the rest 14 cycles. On the other hand, ΔR_m for GDL 35BC increased gradually for the first 27 cycles from 0 mΩ to 5.6 mΩ and became stable thereafter.

It can be induced from these results that the degradation process related to mass transport for the PEMFC using GDL 10BA occurred rapidly and finished after a small number of freezing cycles. The PEMFC using GDL 35BC showed a relatively smaller degree of degradation in mass transport than GDL 10BA, but it required a longer time to finish. Generally, the mass transport resistance is related to the interface between the catalyst layer and GDL and the characteristics of GDL itself. GDL 10BA has a weaker contact force with the catalyst layer than GDL 35BC because the former does not have MPL. Thus, ice-sheet formation between the catalyst layer and GDL can weaken the physical contact between them. Once any space is generated by the volumetric expansion of ice, water will be stored in the big pores. Given that GDL is composed of small pores some of which are hydrophobic, the water in the hydrophilic big pores will not be easily removed through GDL since the big pores are in contact with the catalyst layer that has hydrophilic ionomers. On the other hand, GDL 35BC has MPL which good contact with the catalyst layer. In addition, MPL has such small hydrophobic pores whose average diameter is 250 nm [6] that the amount of water existing in that region should be much less than that for GDL 10BA. This causes a gradual increase in ΔR_m.

It was mentioned that the fluctuation was mainly caused by the Pt area loss and recovery. It was seen that R_t decreased a lot when comparing Fig. 12(c) and (d). Because of the recovery of the effective Pt area, the performance also was recovered. However, ΔR_m showed little variation between the 14th and 23rd cycles. These results support that the fluctuation bears little relation to the mass transport resistance, and that the degradation in mass transport is irreversible.

4. Conclusion

The effect of MPL was investigated in repetitive freezing conditions. An in situ observation of performance degradation and EIS measurement was carried out for two kinds of GDL. For PEMFCs using either GDL 35BC or GDL 10BA, the performance degradation occurred with an increasing number of freezing cycles. OCV was not affected by the number of freezing cycles, but the performance degradation was intensified with increasing current density. The performance degradation was not gradual but fluctuating with the freezing cycles, and the amplitude of the fluctuation was larger at higher current densities. Damage on the catalyst layer took place earlier when GDL with MPL was used because the membrane and catalyst layer kept more water even after finishing the operation. This also explains the reduction in the fluctuation of the performance with an increase in the number of freezing cycles for the PEMFC with GDL 35BC.

The EIS results provided more detailed information about the degradation. The ohmic resistance, R_Ω, showed little variation with repeated freezing cycles for GDL 10BA, but it showed an increasing trend for GDL 35BC. The effect of MPL, which yields high electrical conductivity and high membrane hydration, was reduced by the freezing cycles. The value of ΔR_m was inferred to capture the effect of the mass transport loss. At a high current density, ΔR_m for GDL 10BA increased drastically at the beginning of the repetitive freezing cycles; however, the increase in the mass transport resistance ceased in the ninth cycle. The degradation of mass transport for GDL 35BC increased gradually and did not show its terminal value until the 27th freezing cycle. Consequently, from the point of view that MPL reduces the ohmic resistance, MPL was effective until the first 40 freezing cycles. But the effect disappeared afterwards. On the other hand, from the point of view that MPL enhances mass transport, it delayed the degradation of mass transport and kept the terminal value of ΔR_m below that of GDL without MPL.

Acknowledgements

This work was supported by Mid-career Researcher Program through NRF grant funded by the MEST (No. 2009-0086642). It was also supported by a Korea University Grant.

References

[1] Z. Qi, A. Kaufman, J. Power Sources 109 (2002) 38–46.
[2] J. Chen, T. Matsuura, M. Hori, J. Power Sources 131 (2004) 155–161.
[3] G.G. Park, Y.J. Sohn, T.H. Yang, Y.G. Yoon, W.Y. Lee, C.S. Kim, J. Power Sources 131 (2004) 182–187.
[4] U. Pasaogullari, C.Y. Wang, Electrochim. Acta 49 (2004) 4359–4369.
[5] A.Z. Weber, J. Newman, J. Electrochem. Soc. 152 (2005) A677–A688.
[6] U. Pasaogullari, C.Y. Wang, K.S. Chen, J. Electrochem. Soc. 152 (2005) A1574–A1582.
[7] M.V. Williams, H.R. Kunz, J.M. Fenton, J. Electrochem. Soc. 151 (2004) A1617–A1627.
[8] C. Lim, C.Y. Wang, Electrochim. Acta 49 (2004) 4149–4156.
[9] H.K. Atiyeh, K. Karan, B. Peppley, A. Phoenix, E. Halliop, J. Pharoah, J. Power Sources 170 (2007) 111–121.
[10] Q. Yan, H. Toghiani, Y.W. Lee, K. Liang, H. Causey, J. Power Sources 160 (2006) 1242–1250.
[11] E.A. Cho, J.J. Ko, H.Y. Ha, S.A. Hong, K.Y. Lee, T.W. Lim, I.H. Oh, J. Electrochem. Soc. 150 (2003) A1667–A1670.
[12] E.A. Cho, J.J. Ko, H.Y. Ha, S.A. Hong, K.Y. Lee, T.W. Lim, I.H. Oh, J. Electrochem. Soc. 151 (2004) A661–A665.
[13] J. Hou, H. Yu, S. Zhang, S. Sun, H. Wang, B. Yi, P. Ming, J. Power Sources 162 (2006) 513–520.
[14] S. Ge, C.Y. Wang, J. Electrochem. Soc. 154 (2007) B1399–B1406.
[15] S. Kim, M.M. Mench, J. Power Sources 174 (2007) 206–220.
[16] S. Kim, B.K. Ahn, M.M. Mench, J. Power Sources 179 (2008) 140–146.
[17] Y. Lee, Y. Kim, Y. Jang, J.M. Choi, J. Mech. Sci. Technol. 21 (2007) 2188–2195.
[18] Y. Lee, B. Kim, Y. Kim, Int. J. Hydrogen Energy 34 (2009) 1999–2007.
[19] S. Ge, C.Y. Wang, Electrochim. Acta 52 (2007) 4825–4835.
[20] K. Tajiri, Y. Tabuchi, C.Y. Wang, J. Electrochem. Soc. 154 (2007) B147–B152.
[21] V.A. Paganin, C.L.F. Oliveira, E.A. Ticianelli, T.E. Springer, E.R. Gonzalez, Electrochim. Acta 43 (1998) 3761–3766.
[22] S.W. Cha, R. O'Hayre, Y.I. Park, F.B. Prinz, J. Power Sources 161 (2006) 138–142.
[23] X. Yuan, J.C. Sun, M. Blanco, H. Wang, J. Zhang, D.P. Wilkinson, J. Power Sources 161 (2006) 920–928.
[24] A. Hakenjos, M. Zobel, J. Clausnitzer, C. Hebling, J. Power Sources 154 (2006) 360–363.